Imaging and Musculoskeletal Modeling to Investigate the Mechanical Etiology of Patellofemoral Pain

20

Thor F. Besier, Christine Draper, Saikat Pal, Michael Fredericson, Garry Gold, Scott Delp, and Gary Beaupré

[AU1]

20.1 Introduction

20.1.1 Importance of Understanding the Underlying Mechanism of Pain

Despite the wealth of scientific literature regarding the knee extensor mechanism and patellofemoral (PF) pain, the etiology of PF pain is still poorly understood. Accurate clinical assessment and subject-specific treatment plans for patients with PF pain remain a challenge due to the complexity of the extensor mechanism, large variation among subjects, and the multifactorial nature of the syndrome. However, only once the mechanism of pain is properly understood will we be able to develop effective intervention programs to reduce the incidence and severity of this common knee disorder. To this end, the goal of our research is to understand the etiology of PF pain using a novel combination of medical imaging and musculoskeletal modeling.

The subjective nature of pain presents a problem for researchers wishing to understand the mechanism of PF pain. Most of us appreciate that pain can be related to some physical cause and this explains the majority of PF pain research to date, which attempts to associate symptoms with some mechanical variable(s). However, despite the wealth of literature investigating the mechanical etiology of PF pain, mechanical variables remain poor predictors of symptoms. This is most likely due to our inability to accurately measure or estimate the mechanical variable(s) of interest, as well as our difficulty to quantify and standardize levels of pain.

Regardless of psychological state, it is fair to assume that the *initial onset* of PF pain has some pathophysiological origin. That is, some noxious stimulus (mechanical or chemical) produces a response from a nociceptor that elicits the sensation of pain. This point perhaps necessitates the differentiation between patients with acute symptoms and those with chronic pain, who might experience pain via different pathways (pathophysiological vs psychological). There are many tissues comprising and surrounding the PF joint that have a rich nerve supply and thus have the potential to be a source of pain. These include subchondral bone, infrapatellar fat pad, quadriceps tendon, patellar ligament, synovium, the medial and lateral retinaculum, and the medial and lateral patellar ligaments. These structures, individually, or in combination, may cause pain.[10,22,23,26,55,66,68]

One common hypothesis for the mechanical etiology of pain is that localized stresses transmitted through cartilage excite nociceptors in the subchondral bone.[24] Mineralized bone has a rich sensory and sympathetic innervation[45] and the presence of substance-P fibers (pain receptors) in the subchondral plate of human patellae[68] support this bone stress–pain relationship. However, support for this relationship in patients with PF pain has proven difficult, as neither stress nor pain can be easily quantified. Several factors can contribute to increased subchondral bone stress, as illustrated in Fig. 20.1.

The central focus of our research to date has been to determine if patients with PF pain exhibit increased cartilage stress compared to pain-free controls. We have selected stress as the mechanical variable of interest as stress is a normalized quantity of force (force/area)

T.F. Besier (✉)
Department of Orthopaedics,
Stanford University, Stanford, CA, USA
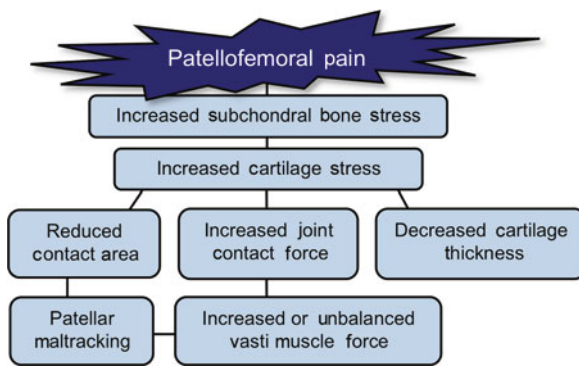e-mail: besier@stanford.edu

Fig. 20.1 Factors that may contribute to increased cartilage and subchondral bone stress and patellofemoral pain

that can be compared across individuals, taking into account joint size and articulating geometry. Mechanical stress is also related to the physical stimuli imposed at the cellular level, which is responsible for maintenance and adaptation of skeletal tissues.[14] The following chapter provides an overview of our imaging and musculoskeletal modeling work to investigate factors influencing cartilage and bone stress and how these factors might contribute to PF pain.

20.2 Imaging the Patellofemoral Joint

20.2.1 Upright Weight-Bearing Imaging of the Patellofemoral Joint

Patellofemoral pain is typically exacerbated by activities that involve large knee extension loads such as stair climbing, squatting, and running. However, examination of the PF joint with computed tomography (CT) and magnetic resonance imaging (MRI) is commonly performed with the patient in a supine orientation with little or no load applied to the joint. To image the joint under physiologic, loaded conditions we developed MR imaging sequences for an open-bore MRI scanner (0.5T GE Signa SP), which enables volumetric scans of the knee to be taken with the patient in an upright, weight-bearing posture.[27] A custom backrest enables patients to remain still for the 2:30 min duration of the scan and the patient can squat to 60° of knee flexion with their knee at the center of the magnet (Fig. 20.2a). The volumetric images from these scans can be used to measure contact area of the PF joint

(Fig. 20.2b) and determine the three-dimensional orientation of the patella with respect to the femur (Fig. 20.2c).

20.2.1.1 Contact Area Measurements

Using this novel weight-bearing imaging modality, we asked several scientific questions. Firstly, what are the ranges of PF contact areas in a healthy, pain-free population of males and females? Secondly, is there a gender difference in contact area when normalizing for patella size? And third, what is the effect of upright, weight-bearing load on contact area?

To answer our first question, we measured contact areas of the PF joint at 0°, 30°, and 60° of knee flexion in eight male and eight female pain-free subjects.[6] Males displayed mean PF joint contact areas of 210, 414, and 520 mm^2 at 0, 30, and 60° of knee flexion, respectively in the low load condition. These values were 20–30% larger than those previously reported in the literature from non-weight bearing MR images or pressure-sensitive film in cadavers. Unloaded contact areas of female subjects were similar to males at full extension (0°), but smaller at 30° and 60°, with mean values of 269 and 396 mm^2, respectively. This was not surprising given that females are generally smaller than males. We therefore normalized the contact area measurements by the dimensions of the patella (height × width). After normalizing for patella area, there were no longer any differences in contact areas between genders. Although females are more likely to develop PF pain, these data suggest that patella size is not a predisposing risk factor.

To determine the influence of load on PF joint contact area, we imaged the joint under full weight-bearing load and compared these values to a low load condition with the subject upright and resting on the seat of the backrest (~0.15 body weight through both knees). Contact areas under weight-bearing conditions increased an average of 24% compared to the low load condition (Fig. 20.3), illustrating the importance of imaging the joint in an upright weight-bearing orientation. Differences between the low load and weight-bearing load can be due to both cartilage deformation as well as altered orientation of the patella within the trochlear groove. The large standard deviations in these measures indicate that some subjects had much greater changes in contact area compared to others.
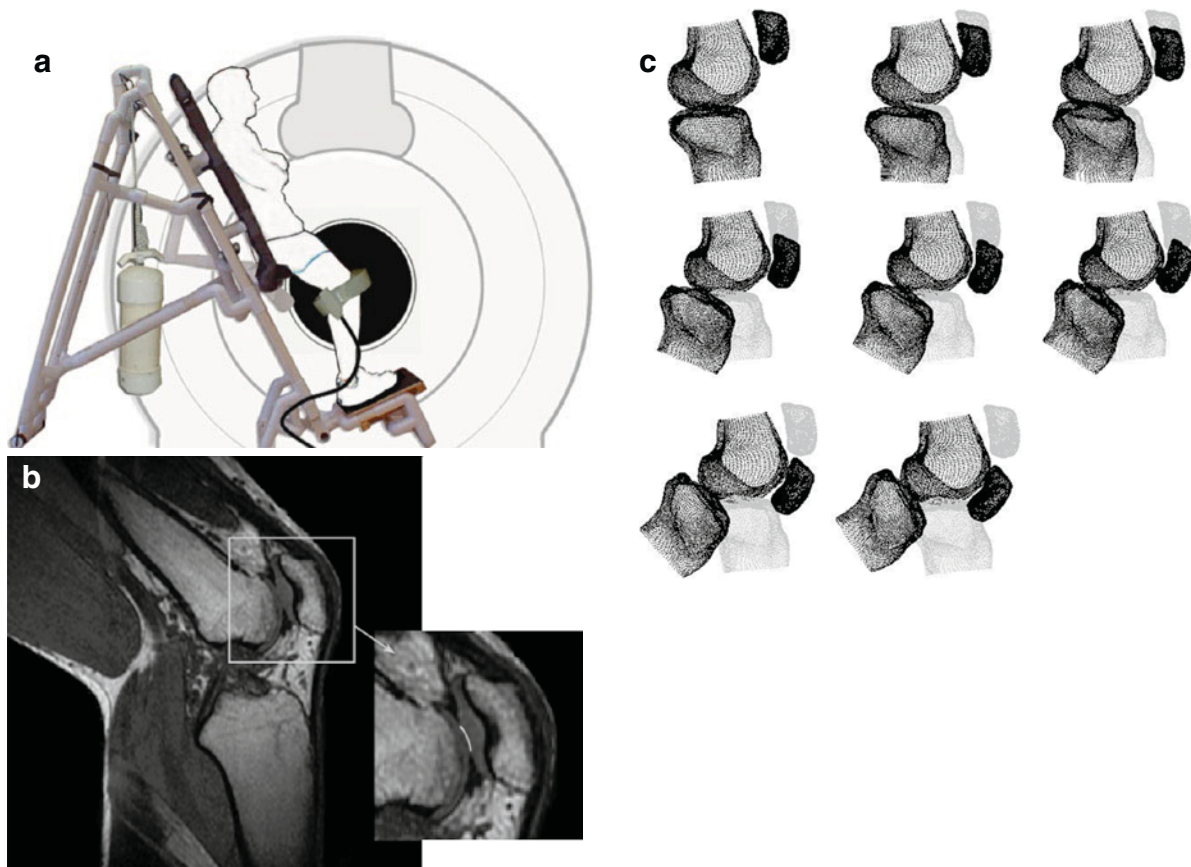
[AU2]

Fig. 20.2 Upright weight-bearing imaging in the 0.5T GE Signa MRI scanner. The custom backrest (**a**) enables subjects to remain still during the scan, while supporting ~90% of their body weight. The backrest can be locked into place and a small seat can be engaged from behind to enable images to be taken under minimal load and no quadriceps activity (~0.15 body weight). Volumetric images of the knee can then be used to determine contact areas (**b**) and the three-dimensional orientation of the patellofemoral joint through different amounts of knee flexion (**c**)
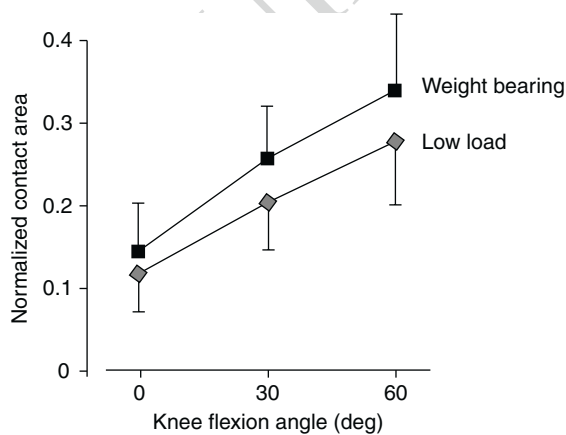

Fig. 20.3 Normalized patellofemoral joint contact areas under loaded and unloaded conditions (Adapted from Besier et al.[5])

20.2.1.2 Cartilage Morphology

High-resolution MR images of the PF joint also enable the assessment of cartilage thickness in the contacting regions of the patella and anterior femur (Fig. 20.4a). Cartilage thickness maps are relevant to tissue stress as thinner cartilage leads to increased stress[41] and it is possible that patients with PF pain have thin cartilage compared to pain-free subjects. To test this hypothesis, we compared PF joint cartilage thickness of 16 pain-free control subjects (eight males and eight females) with 34 patients with PF pain (12 males and 22 females).[19] A young subject population was chosen (28 ± 4 year) to negate any potential influences of cartilage degeneration with aging. We discretized the patella and femur surfaces into three regions of interest (Fig. 20.4c), to represent the different areas of contact
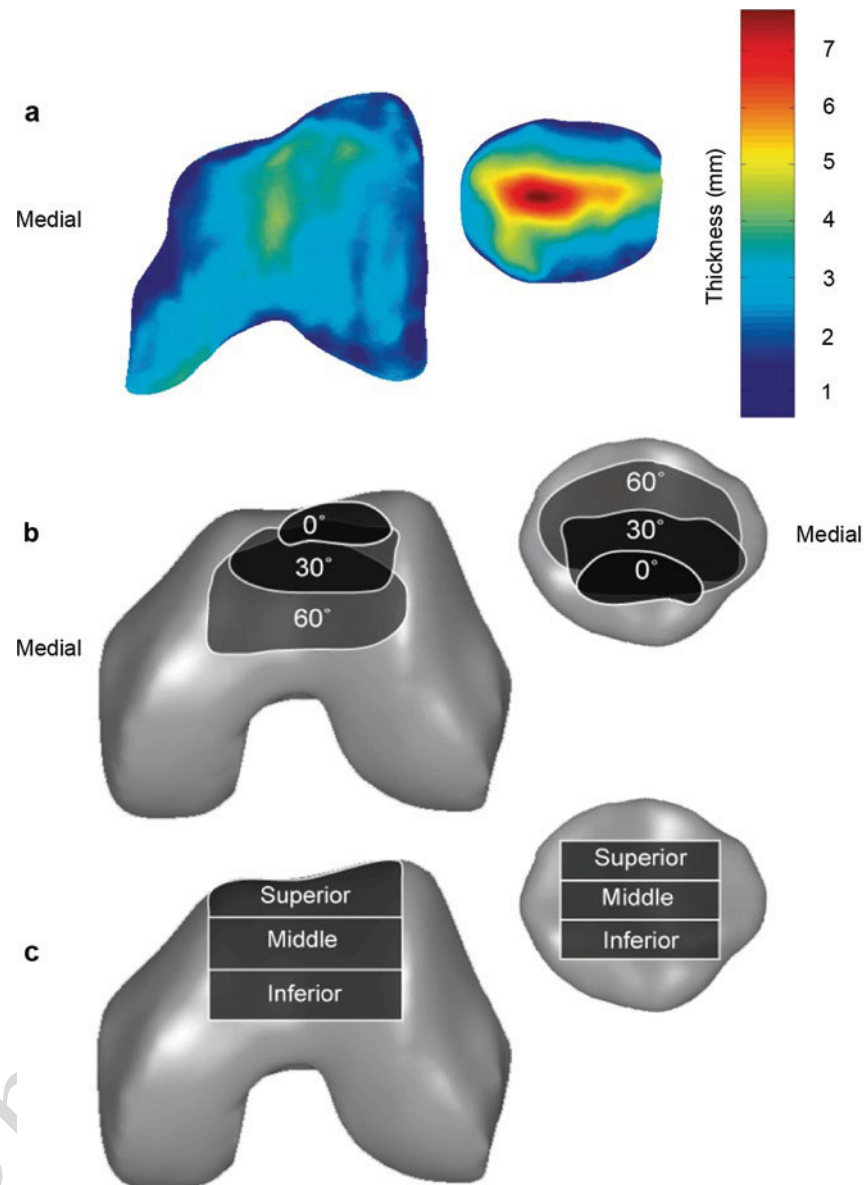
Fig. 20.4 (**a**) Cartilage thickness map of the anterior femur and patella. (**b**) Contact areas corresponding to 0°, 30°, and 60° of knee flexion. (**c**) Discretized regions where cartilage thicknesses were examined (Adapted from Draper et al.[19])

[AU3]

throughout knee flexion (Fig. 20.4b). On average, males had 22% and 23% thicker cartilage than females in the patella and femur, respectively.[19] Male control subjects had 18% greater peak patellar cartilage thickness than males with PF pain; however, we did not detect differences in patellar cartilage thickness between female control subjects and females with PF pain (Fig. 20.5). Femoral cartilage thicknesses were similar between the control and pain groups. The conclusion drawn from this study was that thin patellar cartilage might be one mechanism of PF pain in male subjects, but is unlikely to be a dominant factor in the development of PF pain in females.

One question that arises from this finding is why males with PF pain might have thinner patellar cartilage. The answer to this question is difficult to ascertain, but in a young population that is devoid of degenerative changes, it is likely related to the loading history of the PF joint. The process of endochondral ossification is influenced by the local stresses within the tissue[15] and these stresses during growth and development dictate the thickness of cartilage in adulthood. Animal models also show that extended periods of inactivity can lead to continued endochondral ossification and cartilage thinning.[63] One hypothesis is that individuals who are less active during adolescence and
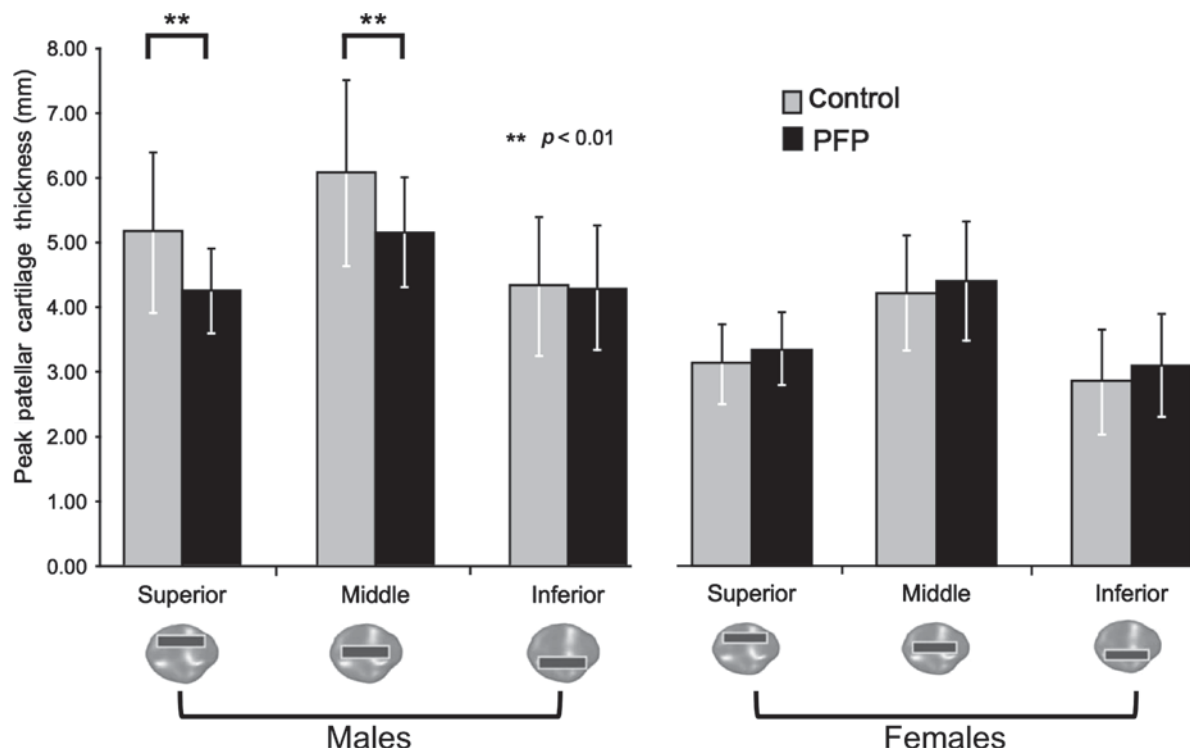
Fig. 20.5 Peak patellar cartilage thickness of males and females with patellofemoral pain (PFP) and a group of pain-free controls. Males with patellofemoral pain had thinner cartilage com-

pared to controls, which might lead to increased cartilage stresses, particularly at deeper angles of knee flexion when the contact is superior and middle

187 early adulthood are predisposed to having thinner car-
188 tilage due to continued endochondral ossification.
189 These individuals might have joints that are poorly
190 suited to distributing large joint loads and perhaps
191 should not take up marathon running at a later age!

20.2.2 Real-Time Magnetic Resonance Imaging to Measure Patellofemoral Joint Kinematics

195 For years, PF pain was ascribed in the presence of
196 malalignment,[36,47] defined as abnormal patellar track-
197 ing and believed to result in overload of the lateral
198 retinaculum and subchondral bone.[25] Malalignment
199 continues to be the focus of many researchers and is
200 typically defined by lateral displacement or lateral tilt
201 of the patella with respect to the femur, both being
202 more pronounced in extension and low load conditions.
203 Maltracking can result from altered femoral rota-
204 tion,[54,58] poor joint articulation[1,65] or abnormal recruit-
205 ment of the vasti muscles.[17,64,67] Recent advancements

206 in medical imaging technologies are permitting a more
207 accurate description of the kinematics of the patell-
208 ofemoral joint in supine unloaded,[56,69] supine low
209 load[46,53] and upright loaded configurations.[20,51,61]
210 However, despite these recent advancements, there is
211 no clear consensus regarding the definition of mal-
212 tracking, the cause of maltracking, or the relationship
213 between maltracking and pain. To begin exploring
214 these relationships, we implemented real-time MR
215 imaging in our 0.5T Signa open-bore MRI scanner to
216 image the PF joint under dynamic upright weight-
217 bearing motion (Fig. 20.6).

218   Real-time image acquisition produces a time series
219 of single image slices.[2] The imaging plane can be con-
220 tinuously defined and updated in real time to follow an
221 object if out-of-plane motion occurs. Real-time MRI
222 can acquire a plane of image data quickly with recon-
223 structed image display rates of 24 frames/s.[50] This high
224 rate of image acquisition and display minimizes the risk
225 of muscle fatigue during highly loaded motions, allow-
226 ing data to be obtained under weight-bearing conditions.
227 We first established the feasibility of using real-time
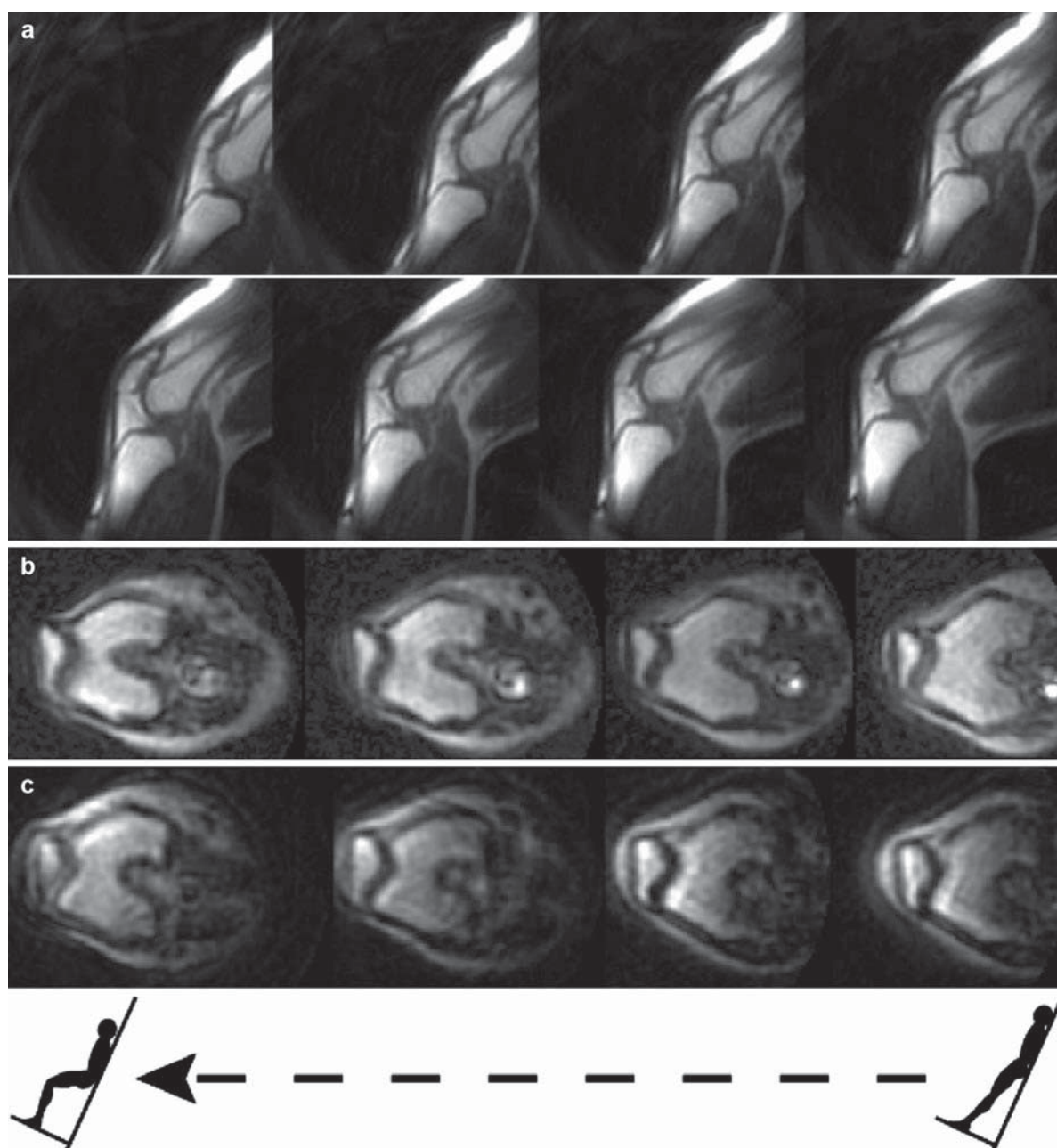228 MRI to measure joint motion using an MR-compatible

Fig. 20.6 (**a**) Sample sagittal plane real-time MR images of patellofemoral joint during weight-bearing knee flexion. (**b**) Axial images from healthy, pain-free control and (**c**) axial images from a subject with patellofemoral pain

motion phantom with a known and repeatable movement trajectory.[21] In the 0.5T open-bore MRI scanner, we measured the movement of the phantom to within 2 mm for movement speeds of up to 38 mm/s, which corresponds to ~22°/s of knee joint flexion.[21] A limitation of these real-time MR imaging acquisitions is that they cannot be used to obtain kinematic measurements during fast velocities or in three dimensions. Faster image acquisition can be achieved in scanners with greater field strengths (e.g. 1.5 or 3.0T clinical scanners); however, the closed-bore designs of these scanners do not permit upright, weight-bearing postures.

To characterize PF maltracking, we measured weight-bearing axial-plane PF joint kinematics in 13 pain-free females and 23 females diagnosed with PF pain. We assessed the lateral displacement of the patella using a bisect offset index and the lateral rotation using a patellar tilt angle (Fig. 20.7). We found that, on average, females with PF pain exhibited a 10% increase in bisect offset and a 6° increase in patellar tilt compared to pain-free controls.[20] The greatest kinematic differences between groups occurred, as expected, near full extension. Importantly, there was a large variation in the types of maltracking in the pain subjects (Fig. 20.8), including a subset of patients (*n* = 5/23, ~22%) with kinematics no different from controls. These results suggest that weight-bearing maltracking may be related to pain in some subjects, but distinct subgroups of patients with different maltracking patterns exist and it is important to recognize that the underlying mechanism of pain may be different in each subgroup. The implication of these results is that accurate classification of patients is needed for effective treatment.

If imaging modalities are going to be useful for future classification and treatment of PF patients, it is important to understand the importance of imaging under upright, weight-bearing conditions. To address this issue, we compared supine, non-weight-bearing and upright, weight-bearing patellofemoral joint kinematics in a group of 20 subjects diagnosed with PF pain. In subjects with patellar maltracking, the patella translated more laterally during upright, weight-bearing knee
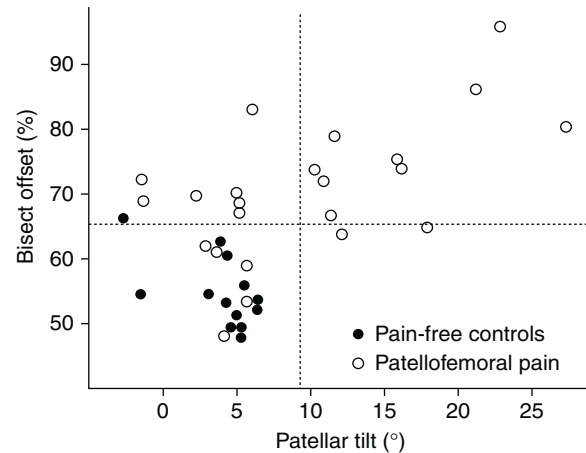
[AU4]

Fig. 20.7

Fig. 20.8 Relationship between bisect offset and patellar tilt at full extension in pain-free controls (*solid circles*) and patellofemoral pain subjects (*hollow circles*). The *dashed lines* represent two standard deviations above the average bisect offset and tilt of the pain-free subjects and were used as thresholds to identify subjects with abnormal patellofemoral joint kinematics (Adapted from Draper et al.[19])

extension for knee flexion angles between 25 and 30°. However, in subjects without maltracking, the patella translated more laterally during supine, non-weight-bearing knee extension for knee flexion angles between 0° and 8°. These results suggest that measurements of patellar tracking performed under non-weight-bearing conditions do not completely reflect weight-bearing joint motion and as a result, clinical diagnosis of patellar maltracking may be more relevant if weight-bearing joint alignment or motion is taken into account. Unfortunately, the majority of clinical MR and CT-based imaging modalities require patients to be supine with little or no load applied to the knee. In our current work, we are assessing the use of upright, static weight-bearing X-ray[11] to assess patellar maltracking and determine the ability of this accessible imaging modality to differentiate lateral maltrackers and non-lateral maltrackers.

20.2.2.1 Influence of Bracing

Using our real-time MR imaging protocol, we evaluated the efficacy of a patellar stabilizing brace and a patellar sleeve in restoring normal joint kinematics. The reduction in bisect offset provided by the brace (6% at full extension) was larger than that provided by the sleeve (4% at full extension) for knee flexion angles between 0° and 60°.[20] Similarly, the brace reduced

patellar tilt by 4° at full extension, while we detected no changes in patellar tilt with application of the knee sleeve. While the brace reduced abnormal patellar kinematics, it did not completely restore normal PF joint motion. An important side result that highlights the need for accurate diagnosis and subject-specific treatment was that PF pain patients with maltracking had greater decreases in both bisect offset and lateral tilt of the patella with brace and sleeve application than PF pain patients with normal PF joint motion. For instance, in patients with abnormal bisect offset, the brace and sleeve reduced bisect offset by 8% and 6%, respectively, whereas in patients with normal bisect offset, the brace and sleeve had no effect on the lateral motion of the patella. Similarly, the brace reduced patellar tilt by 5° more in patients with excessive lateral tilt compared to those with normal patellar tilt.

The clinical implications of this work are that patients with PF pain can be classified into subgroups based upon their PF joint kinematics, and these subgroups are likely to respond differently to different treatment strategies. Accurate assessment of patellar maltracking in a clinical setting would therefore be beneficial for prescribing specific treatment; however, this remains a challenge. In our previous study, the clinical assessment of 8 out of 23 subjects did not correlate with weight-bearing patellar tracking. It remains to be seen whether patients classified as having maltracking also have increased stress in the PF joint, but this will be the focus of our modeling efforts in the near future.

20.2.3 PET–CT Imaging to Understand Tissue Metabolic Response

Ultimately, our goal is to use computational models to predict clinical outcomes from interventions and correlate tissue-level stresses with pain and function. In mineralized bone, areas with high metabolic activity receive the richest sensory and sympathetic innervation, and therefore play an important role in the generation of skeletal pain.[45,57] Quantifying this metabolic activity with functional imaging techniques might offer us a biological metric of bone-related PF pain that we can use to compare with mechanical stresses. Positron Emission Tomography (PET) and ^{99m}Tc-MDP bone scintigraphy (bone scans) are two functional imaging modalities that can be used to highlight areas of increased bone metabolic activity and remodeling, in response to local mechanical stresses or injury within the tissue.

While ^{99m}Tc-MDP bone scintigraphy has provided valuable insights about potential alterations in bone remodeling activity in the PF pain population,[12,33,44,49] ^{18}F-NaF PET/CT is a technique that offers several advantages. For example, compared to traditional bone scans, the spatial resolution of the PET scan is better, the ratio of bone uptake to soft tissue uptake is greater, and the ability to collect PET and CT data at the same time enables accurate anatomical localization of tracer uptake. Traditionally, ^{18}F-NaF PET has been used in the field of oncology; however, recent studies have suggested that ^{18}F-NaF PET is promising for the evaluation of orthopedic conditions, such as in the assessment of bone fracture healing[35] and the identification of sources of back pain.[42] These relationships exist as ^{18}F localizes in areas of bone mineralization or newly exposed mineralized surface, indicating regions of both osteoblastic and osteoclastic activity.[62]

We performed a preliminary study and acquired MR and ^{18}F-NaF PET/CT images of patients with chronic PF pain (>1 year) to assess the regions of bone metabolic activity and determine whether changes in MR signal intensity correlated to ^{18}F uptake. We found increased bone metabolic activity in the patella and/or trochlea of a number of the painful knees (Fig. 20.9).

The most common location of increased metabolic activity was the subchondral region on the lateral facet of the patella. In general, abnormalities in the bone and cartilage detected by MRI (e.g. subchondral cysts, bone marrow edema, cartilage damage) correlated with increased tracer uptake in the ^{18}F-NaF PET/CT images. However, there were a number of regions of increased tracer uptake, indicating increased bone metabolic activity that did not have any structural damage detected by MRI (Fig. 20.10). These preliminary findings suggest that ^{18}F-NaF PET/CT and MRI provide different information about the joint and perhaps ^{18}F-NaF PET/CT can be used to detect early changes in metabolic activity prior to the development of structural damage in the bones and cartilage. We hypothesize that regions of increased metabolic activity in the bone of PF pain patients correlate to regions of increased mechanical stresses in the tissue, which are also related to the development of pain. To test this hypothesis, we have developed a musculoskeletal

Fig. 20.9 Co-registered axial PET/CT image of a unilateral chronic PF pain patient (Male, age 32, characterized with abnormal weight-bearing bisect offset index at full extension). The superimposed CT image enables accurate localization of the PET hotspot, in this case within the apex of the left patella, which was consistent with the area of pain
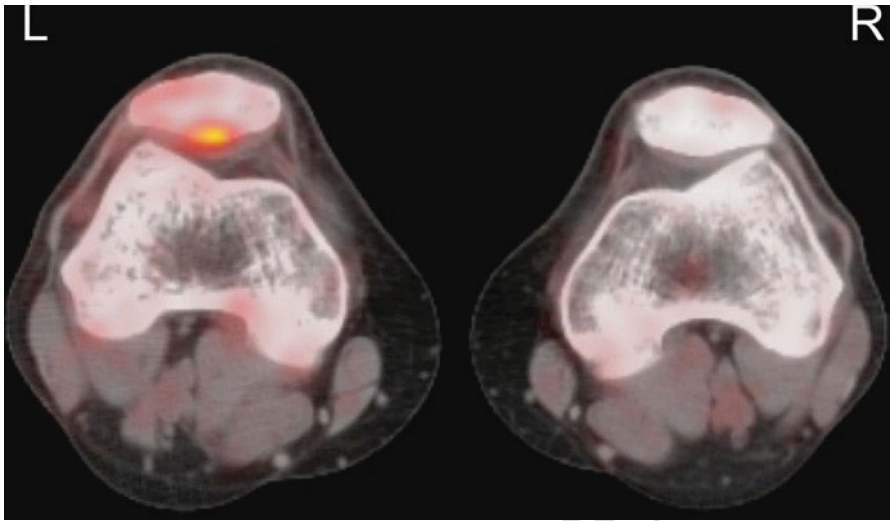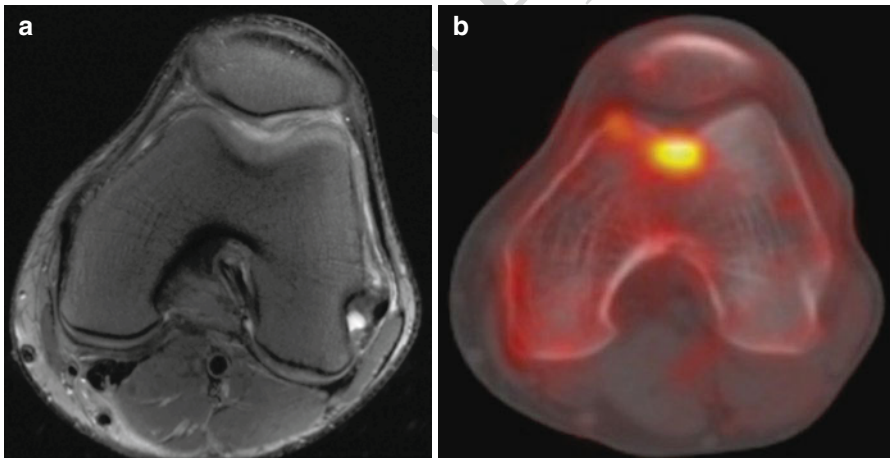
Fig. 20.10 Axial MRI of chronic PF pain patient (**a**), showing no abnormalities within bone or cartilage of the PF joint. Corresponding PET hotspot in the same subject (**b**), indicating areas of high metabolic activity

modeling framework for estimating the mechanical stresses throughout bone and cartilage of the PF joint.

20.3 Musculoskeletal Modeling of the Patellofemoral Joint

To test the hypothesis that patients with PF pain have elevated cartilage and subchondral bone stress compared to pain-free controls, one would ideally take experimental measures of cartilage and bone stresses in a patient population during various dynamic activities. However, direct measurement of in vivo tissue stresses is not feasible, so we must rely on computational methods to estimate these mechanical variables.

Estimating the stresses throughout articular cartilage, bone, and surrounding soft tissues of the PF joint requires knowledge of several factors, including: the loads applied to the tissue; the articulating geometry of the joint; the orientation and position of the joint when the loads are applied; and the morphology and material properties of the different tissues. To capture these complex relationships, we use the finite element method, a numerical technique that enables the calculation of internal tissue stresses, given the joint loads, geometry, and material properties of the different tissues. The accuracy and validity of the finite element method comes from having appropriate material properties and carefully selected loads and boundary conditions. This section briefly describes the work we have performed to create patient-specific finite element

419 models of the PF joint to estimate in vivo cartilage and
420 bone stresses.[8]

421   Our modeling framework consists of several com-
422 ponents, each of which will be described in more detail
423 below:

424 1. Defining the geometry and morphology of the vari-
425   ous tissues
426 2. Defining the material properties of the tissues
427 3. Prescribing the joint orientation/kinematics
428 4. Estimating muscle forces using an EMG-driven
429   model
430 5. Simulation and validation

20.3.1 Defining the Geometry and Morphology of the Various Tissues

433 To define the geometry and morphology of the various
434 tissues of the PF joint, we take high-resolution MR
435 images of the knee. Typically, these are sagittal plane
436 images of the knee using a fat-suppressed spoiled gra-
437 dient echo sequence in a 1.5-T or 3.0-T closed-bore
438 MR scanner (refer to[19] for scan details, Fig. 20.11a).
439 During this scan, the subject is supine with the knee

440 fully extended to ensure the cartilage is imaged in an
441 undeformed state. The MR images are then manually
442 segmented with smooth splines to obtain a three-dimen-
443 sional point cloud of the femur, tibia, and patellar,
444 including the articular cartilage. The quadriceps ten-
445 don, patellar tendon, and suprapatellar fat pad are also
446 segmented from these images (Fig. 20.11a). Triangulated
447 surfaces are then fit to the point clouds using a
448 commercial software package (Geomagic, Research
449 Triangle Park, NC). We then represent each structure as
450 three-dimensional continuum elements with appropri-
451 ate material properties (see below). To mimic the phys-
452 iologic tendon lines-of-action at the patellar, we
453 represent the quadriceps and patellar tendon as hexa-
454 hedral continuum elements. We also include a supra-
455 trochlear fat pad to facilitate patella cartilage–fat pad
456 interaction at extended knee postures (Fig. 20.11a, b,
457 gray arrow). To replicate the physiologic medial–lat-
458 eral constraint at the patella, the medial PF ligament is
459 included as 2D composite elements. Contact is defined
460 between the relevant structures to enable wrapping of
461 the tendons around bone–cartilage–fat pad construct.
462 Three-dimensional continuum element representations
463 of the patella and the distal femur are also defined to
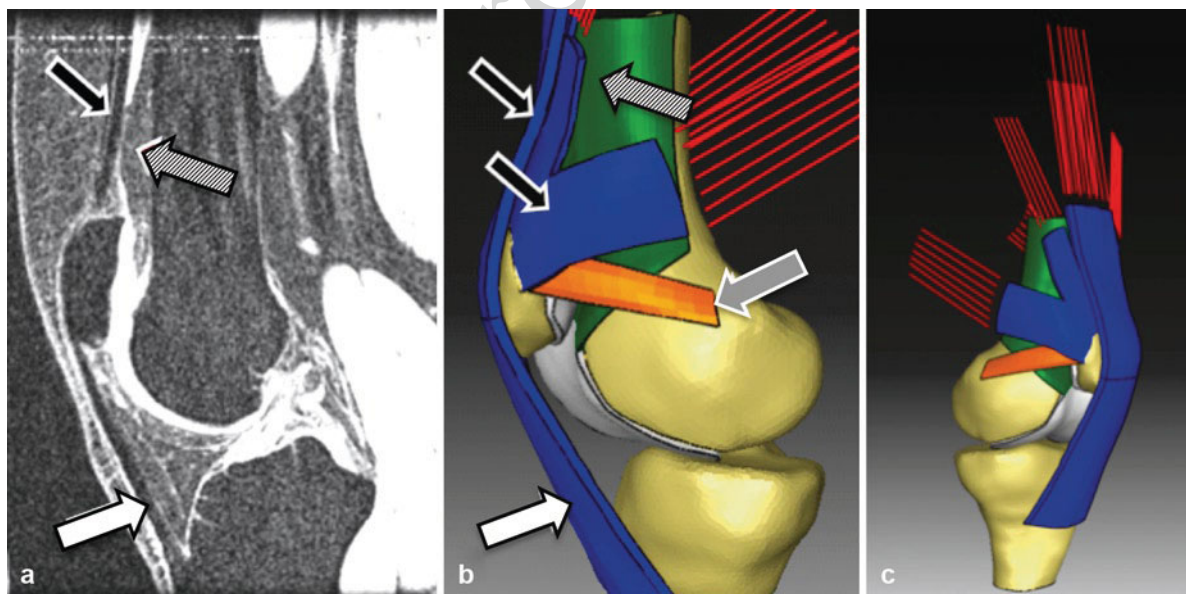464 facilitate stress calculations throughout the bone.

Fig. 20.11 Sagittal MR image (**a**) and corresponding finite ele-
ment model (**b**, **c**) of the patellofemoral joint. The patellar liga-
ment (*white arrows*) and quadriceps tendon (*black arrows*) were
represented as nonlinear fiber-reinforced solid elements, while
the medial patellofemoral ligament (*gray arrow*) was modeled
using 2D composite elements. Articular cartilage and supra-
trochlear fat pad (*striped arrows*) were modeled as linear elastic
solids

20.3.2 Defining the Material Properties of the Tissues

Describing the deformations and stresses throughout a tissue under a given load requires knowledge of the material properties of the tissue. In the finite element method, a continuum approach that describes the overall, macroscopic behavior of the tissue is typically used and these material properties are assigned to each element within the mesh. In its simplest form, each element of a discretized tissue is assigned the same material property, regardless of the direction of loading (isotropic), which includes a stiffness, or elastic modulus, and a Poisson's ratio (describing the ratio of expansion or contraction of a material under compressive or tensile load). Although most biological tissues do not behave as a linear elastic isotropic material, this simple approximation can often describe a tissue's behavior under certain loading conditions. For example, during dynamic loading scenarios such as walking and running, cartilage can be adequately modeled as a linear elastic material due to its elastic response under loads at frequencies greater than 0.1 Hz.[34] The selection of appropriate material properties is therefore dependent on the intended loading scenarios. The models presented in this chapter use a simplified linear elastic material model to describe cartilage mechanical behavior (elastic modulus of 6 MPa and Poisson ratio of 0.47).

There is tremendous focus in the medical imaging community to develop non-invasive methods to estimate material properties of biological tissues. Articular cartilage has received much of this focus in an attempt to detect early degenerative changes and characterize tissue health. Certain parameters measured from an MRI scan of cartilage are known to correlate with the microscopic constituents of the tissue (e.g. T_1 and T_2 relaxation times correlate to proteoglycan and collagen content, respectively), which in turn correlate to the macroscopic material properties.[40] Although outside the scope of this book chapter, our group has a history of developing novel MR imaging sequences for cartilage[28–32] and we are currently exploring the relationship between cartilage imaging (T1rho and sodium imaging) and cartilage mechanical properties.[37] Our aim is to estimate material properties of cartilage using MRI and assign these properties to our finite element simulations.

To describe the material properties for bone, we perform a CT scan to define a radiographic measure of density (measured in Hounsfield units), which can be converted to regional specific bone apparent density.[38,60] This information is mapped onto the finite element mesh[39] and each element in the mesh assigned an appropriate elastic modulus based on the measured bone apparent density (Fig. 20.12). In this case, we model bone as a linear elastic solid.

Describing material properties for tendinous structures is problematic, as the tensile loading response of a tendon is greatly influenced by its resting slack length, which is difficult to measure in vivo. Our approach is to model the quadriceps and patellar tendon as a non-linear hyper-elastic material based on experimental data,[59] as reported by Baldwin et al.[3] The

[AU2]

Fig. 20.12 Axial CT image of chronic PF pain patient illustrating variation in bone mineral density. Color coding on right shows most dense bone (*red*) in the anterior aspect of the patella as well as the lateral facet of the patella
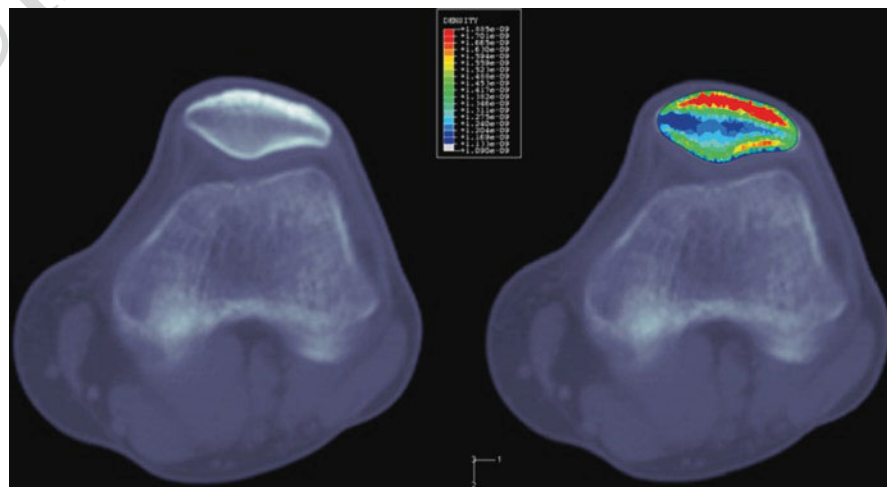
resting tendon length and stiffness profile can then be 'tuned' to match vertical displacement data of the patella under weight-bearing load to ensure the correct displacement of the patellar tendon. A linear elastic material model adapted from tensile testing[48] is currently used to represent the medial PF ligament.

20.3.3 Prescribing the Joint Orientation/Kinematics

Contact force and stress calculations are extremely sensitive to changes in joint orientation and position, particularly for the PF articulation, which has complex articulating surfaces. Millimeters of translation or a degree of rotation can substantially alter contact at the articulating surface of the PF joint. For this reason, the patella has 6° of freedom in our simulations and is free to move in any direction and settle into a position that satisfies static equilibrium based upon the forces acting on it (i.e. the quadriceps and tendon force and the resulting contact forces). Because the joint is modeled with near-zero friction, the final position of the patella depends on the distribution of quadriceps muscle forces and the contacting geometry. Therefore, it is important to describe the initial orientation of the patella prior to the application of muscle forces. To determine the initial orientation of the joint, we register the bone surface mesh of the femur, tibia, and patella to our three-dimensional weight-bearing MR data sets (Fig. 20.13). This registration is performed using a closest iterative point algorithm, which minimizes the distance between points manually selected on the boundary of the bone ($n = 20$–30) and the surface of the bone mesh. A visual comparison of the model within the image data ensures a close registration of the mesh to the image (Fig. 20.13).

Fig. 20.13 Registration of femur finite element mesh (*upper left*) into upright weight-bearing MR imaging volume (*upper right*). Selecting edges of the bone within the imaging data set ensures a close match between the model and MR images (*lower images*)
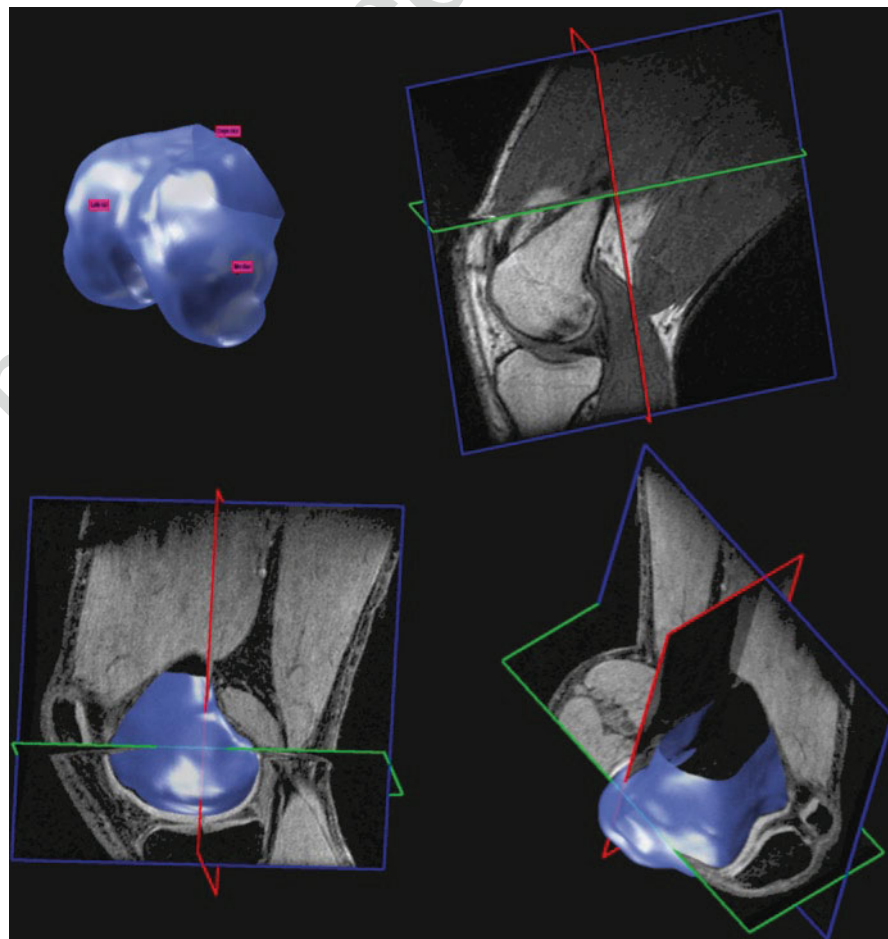
562 Using this registration technique, we can prescribe
563 the initial configuration of the patellofemoral and
564 tibiofemoral joints for each posture that was imaged
565 (typically 0°, 30°, and 60° of knee flexion in our open-
566 bore MR scanner). Describing the tibiofemoral joint
567 orientation is important to ensure an accurate orienta-
568 tion of the patellar tendon and quadriceps tendon. For
569 quasi-static analyses, the tibia and femur remain fixed
570 throughout the simulation as the quadriceps muscle
571 forces are applied. For dynamic analyses, the femur
572 remains fixed and the tibia motion is prescribed. The
573 simulation results presented in this chapter were per-
574 formed as quasi-static analyses.

20.3.4 Estimating Muscle Forces Using an EMG-Driven Model

575
576

577 Quadriceps muscle forces influence the motion of the
578 patella within the trochlear groove, and therefore
579 influence the stress within the cartilage and bone.
580 Accounting for individual muscle activation strategies
581 is important when estimating the distribution of mus-
582 cle forces across the knee joint, particularly in a patho-
583 logical case when altered muscle recruitment patterns
584 are expected. Therefore, we use a musculoskeletal mod-
585 eling method to estimate muscle forces based on elec-
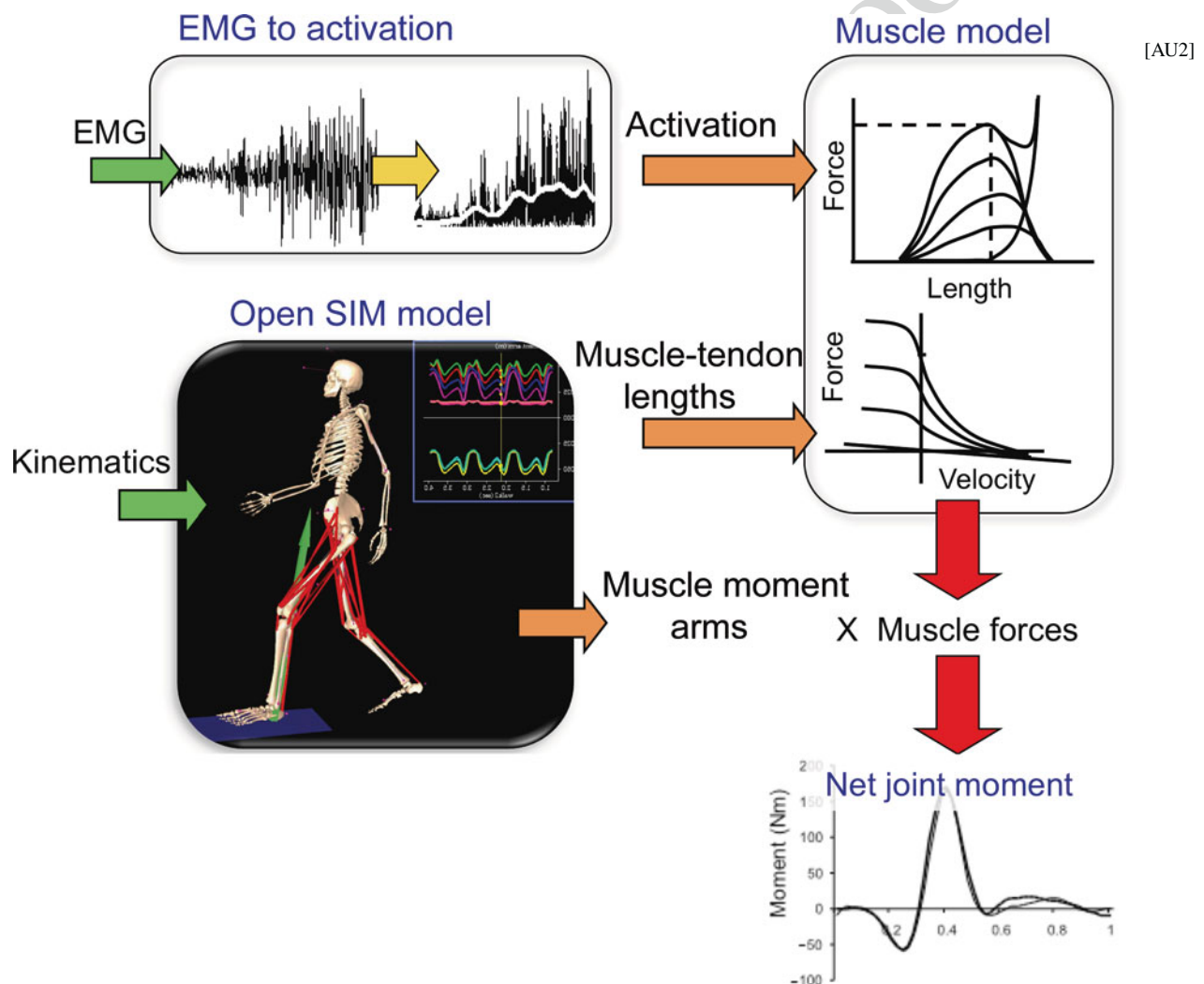586 tromyographic (EMG) signals (4; 13; 43) (Fig. 20.14).

[AU2]

Fig. 20.14 EMG-driven musculoskeletal model overview. Raw EMG and joint kinematics are used to estimate activation and muscle tendon lengths, which are input into a Hill-type muscle model to estimate muscle force. Muscle moment arms calculated from the anatomical model (OpenSIM) are multiplied by the muscle forces to obtain the net joint moment. The net joint moment from the model is compared to the moment calculated from inverse dynamics in a calibration/validation procedure

Briefly, this method takes EMG and joint kinematics (from a standard motion capture experiment) as input to estimate muscle activation and muscle contraction dynamics, respectively. An EMG-to-activation process takes raw EMG and estimates an activation time series, which represents the summed activation of the underlying motor units. This process takes into account the non-linear transfer from EMG to activation as well as the potential non-linearity between muscle force and EMG. The end result of this transfer function is an activation time series, scaled to a maximum voluntary isometric contraction.

We then scale a musculoskeletal model of each individual to match the anthropometry of each subject (from motion capture data). This process is performed using an open-source modeling platform called OpenSim.[18] This scaled anatomical model reproduces the motions of each subject from motion capture data and provides individual muscle tendon lengths and moment arms for each muscle crossing the knee joint. Muscle activation and muscle tendon length are then input to a modified Hill-type muscle model,[43] which estimates individual muscle force, taking into account muscle fiber force-length and force-velocity relationships (Fig. 20.14). The resulting muscle forces are multiplied by their respective moment arms in flexion–extension and the summed muscle moments can be compared to the net joint moment estimated using traditional inverse dynamics analysis. Although muscle forces cannot be measured in vivo, a comparison to the joint moment from inverse dynamics provides a means of indirectly validating the predicted muscle forces. Various parameters in the model are expected to differ among individuals (such as muscle cross-sectional area and non-linear EMG–force relationships) and these parameters can be altered in a calibration process to improve the prediction of the net joint moment. Importantly, this calibration process only occurs on a few select trials. Following calibration, the parameters in the model are not altered and muscle forces and joint moments are predicted equally well for other dynamic tasks, providing some confidence in the predicted muscle forces.[43]

An obvious application of this EMG-driven approach is to investigate the quadriceps muscle force distribution in patients with PF pain during functional activities, such as walking and running. Of particular interest is the relationship between the medial and lateral components of the vastii, as muscle force imbalance is often cited as a cause of patellar maltracking and PF pain. Based on previous literature,[16,64,67] one might hypothesize the relative contribution of the vastus medialis muscle would be less in the patellofemoral pain group compared to pain-free controls during walking and running. To answer this hypothesis, we estimated lower limb muscle forces during walking and running in a group of male and female patients with PF pain ($n = 27$, 16 female; 11 male) and compared the peak quadriceps forces to a group of pain-free controls ($n = 16$, 8 female; 8 male).[7] Surface EMG were collected from seven major muscles crossing the knee joint, including: vastus medialis, vastus lateralis, rectus femoris, biceps femoris, semimembranosus, medial gastrocnemius, and lateral gastrocnemius. We found that subjects with PF pain produced a knee extension moment using the same distribution of quadriceps forces as pain-free individuals during walking and running, which did not support our hypothesis. However, compared to controls, PF pain patients had greater co-contraction of quadriceps and hamstring muscles and greater normalized quadriceps muscle forces during walking. Muscle forces during running were similar between groups, but the net knee extension moment was less in the PF pain group compared to controls. These data suggest that some PF pain patients might experience greater joint contact forces and joint stresses than pain-free subjects by virtue of increased overall quadriceps muscle forces. It is not known whether these muscle force distributions are an adaptation to pain or if they are causative, but one could argue that increased co-contraction around heel strike might improve knee joint stability and help to align the patella within the trochlear groove. On the other hand, increased muscle forces during peak push off would have a detrimental effect of increasing joint contact forces. Whether or not these increased muscle forces lead to increased cartilage or bone stress in these patients remains to be seen, although these data provide valuable input to our finite element simulations, which are capable of answering such questions.

20.3.5 Simulation and Validation

The final stage in our modeling pipeline is to run the finite element simulation and validate the results. As stated previously, during quasi-static analyses the femur and tibia are fixed and the patella is constrained

only by the forces of the quadriceps muscles and patellar tendon and the contact forces from the femur. The quadriceps muscle forces from the EMG-driven model are applied to the quadriceps tendons during the simulation, causing the patella to settle into the trochlear groove until reaching static equilibrium. All our simulations are run using a non-linear finite element solver (ABAQUS, Pawtucket, RI).

One of the most important aspects of using a computational model to investigate a clinical problem is validation. Although we cannot directly validate the model stresses to experimental measures, there are other variables that can be used to validate each simulation. Firstly, contact areas measured from weight-bearing MR images can be compared to those predicted by the simulation. Our initial models generated for 16 healthy, pain-free controls had PF contact areas within 5% of those measured from MRI for 10 of the 16 subjects.[9] Secondly, we can compare the final orientation of the patella to that obtained from the weight-bearing MRI. On average, the patella orientation during the simulation was within $3.7° \pm 5.98°$ of tilt and $4.7° \pm 7.68°$ of rotation of the measured orientation.[9] Discrepancies in contact area and patella orientation can be due to; incorrect estimation of muscle forces, errors in the line of action of the muscles (these simulations did not include wrapping of the quadriceps tendon), and/or the prescribed material properties of the tissue. Our current framework introduces an optimization/calibration scheme to make subtle alterations to the muscle forces and cartilage material properties to enable a closer match between the measured contact areas and patella orientation over a range of squatting postures.

20.3.6 Cartilage and Bone Stresses in the Patellofemoral Joint

The driving question behind much of this work is whether patients with PF pain exhibit cartilage and bone stresses that are greater than pain-free controls. Our final dataset includes 57 PF pain patients and 16 pain-free controls. Of these patients, 22 have undergone PET/CT imaging, so we have the capability of estimating bone stresses and comparing these stresses to metabolic activity. For the other 51 subjects, we will estimate the cartilage stress distributions at the layer of cartilage closest to the subchondral bone and compare stress distributions between PF pain patients and pain-free controls. We would like to conclude this chapter with some interesting findings from our preliminary modeling studies.

Firstly, we have found that cartilage stresses are not intuitively predicted based upon joint kinematics alone,[9] which may seem to contradict conventional wisdom relating to PF biomechanics. The stresses developed throughout the cartilage of the patellofemoral joint are a result of complex interactions between the articulating geometry of the patella and femur, cartilage morphology, cartilage material properties, and the distribution of forces acting on the patella. Variations in each of these parameters may be responsible for the different stress responses that resulted from these simulations. Figure 20.15 illustrates a range of different cartilage stress distributions from five patients with PF pain performing a static squat at 60° of knee flexion. These stress distributions show that peak stress locations are not always located on the lateral facet of the
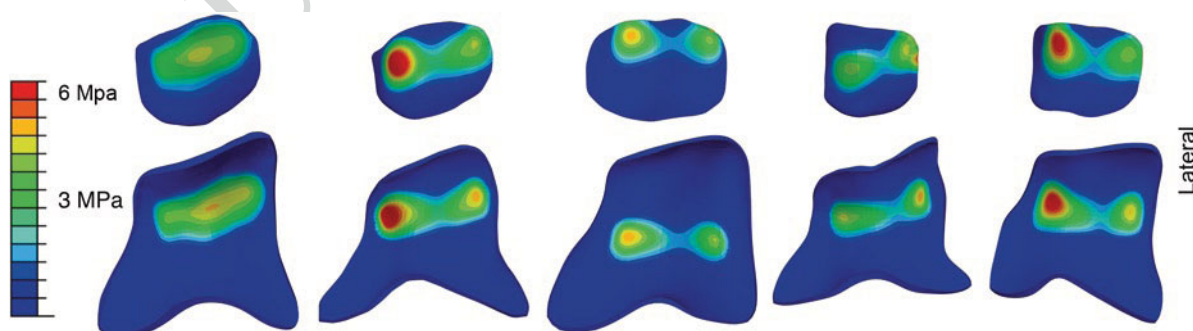

Fig. 20.15 Example hydrostatic stresses in the layer of patellar and femoral cartilage closest to the subchondral bone in five patients with PF pain during a static squat at 60° of knee flexion. Note the varied distribution and magnitudes of peak hydrostatic pressure across this small sample. The lateral aspect of the joint is toward the right on each example. Stress "hot spots" are common on the medial aspect of the PF joint cartilage

PF joint and are often located on the medial facet. These peak stress locations do not necessarily reflect the orientation of the bone, which is typically what we measure when we discuss PF joint kinematics and maltracking. To highlight this point, we performed a series of simulations with our pain-free control data set to determine what effect internal and external rotation of the femur would have on cartilage stress.[9] Some individuals responded to femoral internal rotation with large changes in cartilage stresses, whereas others show little or no change with the same degree of femoral rotation. This insight has clinical relevance, particularly when considering treatment strategies to reduce stress. Assuming that cartilage stresses are related to pain from increased stresses transmitted through the cartilage into the subchondral bone, individuals who are more sensitive to changes in femoral rotation might respond positively to therapies or intervention strategies that focus on controlling femoral rotation. However, subjects who are relatively insensitive to changes in femoral rotation may not respond to any intervention that is designed to alter femoral orientation, such as stretching and strengthening of hip muscles. The modeling framework presented here offers the capability to identify important variables that relate to potential changes in tissue-level stresses and how these stresses might relate to potential joint and cartilage pathology.

Preliminary comparisons between six female PF pain patients and six pain-free controls provide some support that cartilage stresses are related to PF pain. We simulated double-leg squats at 60° of knee flexion and found that peak shear stresses within the femur were 28% greater in PF pain patients compared to controls.[5] However, given the variability across subjects and the different factors that can influence cartilage stress, many more simulations are required to understand the relationship between tissue stress and pain. We are also exploring the use of statistical modeling techniques to account for known variation in model input parameters.[52] These methods will provide us with useful information regarding which parameters have the greatest influence on tissue stresses, thus guiding further interventions on a subject-specific basis.

As stated previously, one of our goals is to correlate tissue stresses to biological measures of pain and function. To this end, we are now comparing bone stresses in the PF joint with PET image intensity, which is an indirect measure of bone metabolic activity. Preliminary findings show good qualitative comparisons between PET signal intensity and mechanical stress within the bone (Fig. 20.16). We hope this work will take us one step closer to understanding the mechanical etiology of PF pain.
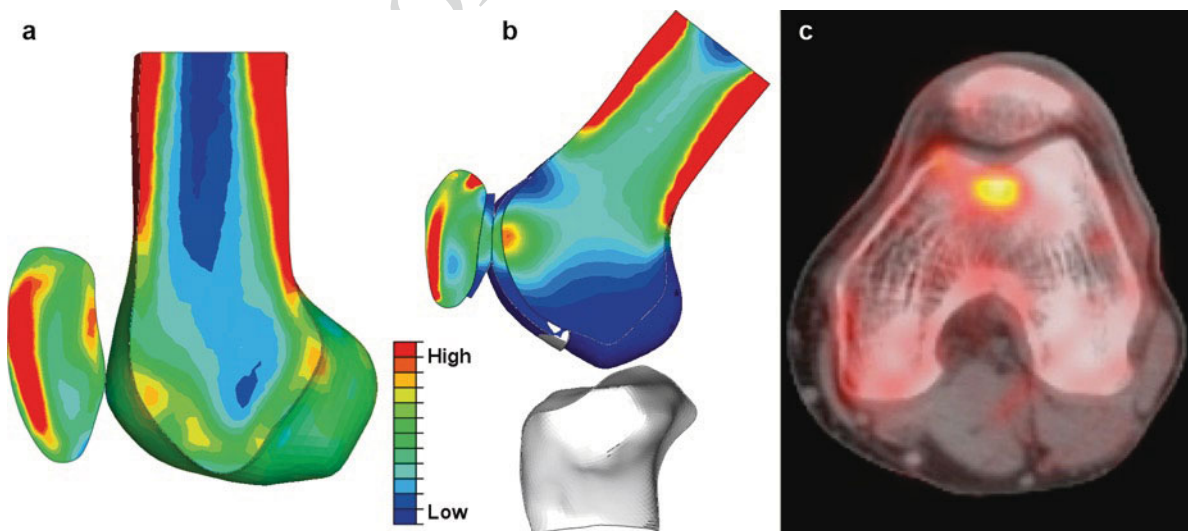

Fig. 20.16 Bone density assignment from CT-based Hounsfield Units (**a**), and predicted bone-cartilage stress from finite element modeling (**b**) during a 60° static squat. Peak subchondral bone stresses in the trochlear of the femur correspond to the hot spot from PET scanning on the same subject (**c**) [AU5]

20.4 Concluding Remarks

The combination of advanced medical imaging and musculoskeletal modeling presented here provides us with a unique set of tools to investigate the complex form and function of the PF joint. In particular, the ability to estimate patient-specific stresses throughout various tissues of the PF joint enables us to test the fundamental hypothesis that the onset and development of PF pain has an underlying mechanical etiology.

References

1. Amis AA. Current concepts on anatomy and biomechanics of patellar stability. *Sports Med Arthrosc*. 2007;15:48-56.
2. Asakawa DS, Nayak KS, Blemker SS, et al. Real-time imaging of skeletal muscle velocity. *J Magn Reson Imaging*. 2003;18:734-739.
3. Baldwin MA, Clary C, Maletsky LP, et al. Verification of predicted specimen-specific natural and implanted patellofemoral kinematics during simulated deep knee bend. *J Biomech*. 2009;42:2341-2348.
4. Besier T, Delp S, Gold G, et al. Influence of quadriceps muscle force distributions on cartilage stresses at the patellofemoral joint during running. In: *American Society of Biomechanics*. Stanford; 2007.
5. Besier T, Delp S, Gold G, et al. Patellofemoral pain subjects display greater femoral cartilage stresses than pain-free controls. In: *Patellofemoral Pain Syndrome: International Research Retreat*. Baltimore: Elsevier; 2009.
6. Besier TF, Draper CE, Gold GE, et al. Patellofemoral joint contact area increases with knee flexion and weight-bearing. *J Orthop Res*. 2005;23:345-350.
7. Besier TF, Fredericson M, Gold GE, et al. Knee muscle forces during walking and running in patellofemoral pain patients and pain-free controls. *J Biomech*. 2009;42:898-905.
8. Besier TF, Gold GE, Beaupre GS, et al. A modeling framework to estimate patellofemoral joint cartilage stress in vivo. *Med Sci Sports Exerc*. 2005;37:1924-1930.
9. Besier TF, Gold GE, Delp SL, et al. The influence of femoral internal and external rotation on cartilage stresses within the patellofemoral joint. *J Orthop Res*. 2008;26:1627-1635.
10. Biedert RM, Sanchis-Alfonso V. Sources of anterior knee pain. *Clin Sports Med*. 2002;21:335-347.
11. Boegård T, Jonsson K. Radiography in osteoarthritis of the knee. *Skeletal Radiol*. 1999;28(11):605-615.
12. Boegard T, Rudling O, Dahlstrom J, et al. Bone scintigraphy in chronic knee pain: comparison with magnetic resonance imaging. *Ann Rheum Dis*. 1999;58:20-26.
13. Buchanan TS, Lloyd DG, Manal K, et al. Estimation of muscle forces and joint moments using a forward-inverse dynamics model. *Med Sci Sports Exerc*. 2005;37:1911-1916.
14. Carter DR, Beaupre GS. *Skeletal Function and Form. Mechanobiology of Skeletal Development, Aging and Regeneration*. Cambridge: Cambridge University Press; 2001.
15. Carter DR, Beaupre GS, Wong M, et al. The mechanobiology of articular cartilage development and degeneration. *Clin Orthop Relat Res*. 2004;427:S69-S77.
16. Cowan SM, Bennell KL, Hodges PW, et al. Delayed onset of electromyographic activity of vastus medialis obliquus relative to vastus lateralis in subjects with patellofemoral pain syndrome. *Arch Phys Med Rehabil*. 2001;82:183-189.
17. Cowan SM, Hodges PW, Bennell KL, et al. Altered vastii recruitment when people with patellofemoral pain syndrome complete a postural task. *Arch Phys Med Rehabil*. 2002;83:989-995.
18. Delp SL, Anderson FC, Arnold AS, et al. OpenSim: open-source software to create and analyze dynamic simulations of movement. *IEEE Trans Biomed Eng*. 2007;54:1940-1950.
19. Draper CE, Besier TF, Gold GE, et al. Is cartilage thickness different in young subjects with and without patellofemoral pain? *Osteoarthritis Cartilage*. 2006;14:931-937.
20. Draper CE, Besier TF, Santos JM, et al. Using real-time MRI to quantify altered joint kinematics in subjects with patellofemoral pain and to evaluate the effects of a patellar brace or sleeve on joint motion. *J Orthop Res*. 2009;27:571-577.
21. Draper CE, Santos JM, Kourtis LC, et al. Feasibility of using real-time MRI to measure joint kinematics in 1.5T and open-bore 0.5T systems. *J Magn Reson Imaging*. 2008;28:158-166.
22. Dye SF, Vaupel GL, Dye CC. Conscious neurosensory mapping of the internal structures of the human knee without intraarticular anesthesia. *Am J Sports Med*. 1998;26:773-777.
23. Fulkerson JP. The etiology of patellofemoral pain in young, active patients: a prospective study. *Clin Orthop Relat Res*. 1983;179:129-133.
24. Fulkerson JP. Mechanical basis for patellofemoral pain and cartilage breakdown. In: Ewing JW, ed. *Articular Cartilage and Knee Joint Function: Basic Science and Arthroscopy*. New York: Raven; 1990:93-101.
25. Fulkerson JP. Diagnosis and treatment of patients with patellofemoral pain. *Am J Sports Med*. 2002;30:447-456.
26. Fulkerson JP, Tennant R, Jaivin JS, et al. Histologic evidence of retinacular nerve injury associated with patellofemoral malalignment. *Clin Orthop Relat Res*. 1985;197:196-205.
27. Gold GE, Besier TF, Draper CE, et al. Weight-bearing MRI of patellofemoral joint cartilage contact area. *J Magn Reson Imaging*. 2004;20:526-530.
28. Gold GE, Burstein D, Dardzinski B, et al. MRI of articular cartilage in OA: novel pulse sequences and compositional/functional markers. *Osteoarthritis Cartilage*. 2006;14(suppl A):A76-A86.
29. Gold GE, Busse RF, Beehler C, et al. Isotropic MRI of the knee with 3D fast spin-echo extended echo-train acquisition (XETA): initial experience. *Am J Roentgenol*. 2007;188:1287-1293.
30. Gold GE, Hargreaves BA, Stevens KJ, et al. Advanced magnetic resonance imaging of articular cartilage. *Orthop Clin North Am*. 2006;37:331-347.
31. Gold GE, Hargreaves BA, Vasanawala SS, et al. Articular cartilage of the knee: evaluation with fluctuating equilibrium MR imaging-initial experience in healthy volunteers. *Radiology*. 2006;238:712-718.

32. Gold GE, Reeder SB, Yu H, et al. Articular cartilage of the knee: rapid three-dimensional MR imaging at 3.0T with IDEAL balanced steady-state free precession – initial experience. *Radiology*. 2006;240:546-551.

33. Hejgaard N, Diemer H. Bone scan in the patellofemoral pain syndrome. *Int Orthop*. 1987;11:29-33.

34. Higginson GR, Snaith JE. The mechanical stiffness of articular cartilage in confined oscillating compression. *Eng Med*. 1979;8:11-14.

35. Hsu WK, Feeley BT, Krenek L, et al. The use of 18F-fluoride and 18F-FDG PET scans to assess fracture healing in a rat femur model. *Eur J Nucl Med Mol Imaging*. 2007;34:1291-1301.

36. Insall J. "Chondromalacia patellae": patellar malalignment syndrome. *Orthop Clin North Am*. 1979;10:117-127.

37. Keenan KE, Kourtis LC, Besier TF, et al. New resource for the computation of cartilage biphasic material properties with the interpolant response surface method. *Comput Methods Biomech Biomed Eng*. 2009;12:415-422.

38. Keller TS. Predicting the compressive mechanical behavior of bone. *J Biomech*. 1994;27:1159-1168.

39. Kourtis LC, Carter DR, Kesari H, et al. A new software tool (VA-BATTS) to calculate bending, axial, torsional and transverse shear stresses within bone cross sections having inhomogeneous material properties. *Comput Methods Biomech Biomed Eng*. 2008;11:463-476.

40. Kurkijarvi JE, Nissi MJ, Kiviranta I, et al. Delayed gadolinium-enhanced MRI of cartilage (dGEMRIC) and T2 characteristics of human knee articular cartilage: topographical variation and relationships to mechanical properties. *Magn Reson Med*. 2004;52:41-46.

41. Li G, Lopez O, Rubash H. Variability of a three-dimensional finite element model constructed using magnetic resonance images of a knee for joint contact stress analysis. *J Biomech Eng*. 2001;123(4):341-346.

42. Lim R, Fahey FH, Drubach LA, et al. Early experience with fluorine-18 sodium fluoride bone PET in young patients with back pain. *J Pediatr Orthop*. 2007;27:277-282.

43. Lloyd DG, Besier TF. An EMG-driven musculoskeletal model to estimate muscle forces and knee joint moments in vivo. *J Biomech*. 2003;36:765-776.

44. Lorberboym M, Ami DB, Zin D, et al. Incremental diagnostic value of 99 mTc methylene diphosphonate bone SPECT in patients with patellofemoral pain disorders. *Nucl Med Commun*. 2003;24:403-410.

45. Mach DB, Rogers SD, Sabino MC, et al. Origins of skeletal pain: sensory and sympathetic innervation of the mouse femur. *Neuroscience*. 2002;113:155-166.

46. MacIntyre NJ, Hill NA, Fellows RA, et al. Patellofemoral joint kinematics in individuals with and without patellofemoral pain syndrome. *J Bone Joint Surg*. 2006;88-A:2596-2605.

47. Merchant AC, Mercer RL, Jacobsen RH, et al. Roentgenographic analysis of patellofemoral congruence. *J Bone Joint Surg*. 1974;56-A:1391-1396.

48. Mountney J, Senavongse W, Amis AA, et al. Tensile strength of the medial patellofemoral ligament before and after repair or reconstruction. *J Bone Joint Surg*. 2005;87-B:36-40.

49. Naslund JE, Odenbring S, Naslund UB, et al. Diffusely increased bone scintigraphic uptake in patellofemoral pain syndrome. *Br J Sports Med*. 2005;39:162-165.

50. Nayak KS, Cunningham CH, Santos JM, et al. Real-time cardiac MRI at 3 tesla. *Magn Reson Med*. 2004;51:655-660.

51. Nha KW, Papannagari R, Gill TJ, et al. In vivo patellar tracking: clinical motions and patellofemoral indices. *J Orthop Res*. 2008;26:1067-1074.

52. Pal S, Beaupre G, Delp S, et al. Variations in muscle forces affect patellofemoral contact areas and cartilage stresses. In: *Patellofemoral Pain Syndrome: International Research Retreat*. Baltimore: Elsevier; 2009.

53. Patel VV, Hall K, Ries M, et al. Magnetic resonance imaging of patellofemoral kinematics with weight-bearing. *J Bone Joint Surg*. 2003;85-A:2419-2424.

54. Powers CM, Ward SR, Fredericson M, et al. Patellofemoral kinematics during weight-bearing and non-weight-bearing knee extension in persons with lateral subluxation of the patella: a preliminary study. *J Orthop Sports Phys Ther*. 2003;33:677-685.

55. Sanchis-Alfonso V, Rosello-Sastre E, Martinez-Sanjuan V. Pathogenesis of anterior knee pain syndrome and functional patellofemoral instability in the active young. *Am J Knee Surg*. 1999;12:29-40.

56. Seisler AR, Sheehan FT. Normative three-dimensional patellofemoral and tibiofemoral kinematics: a dynamic, in vivo study. *IEEE Trans Biomed Eng*. 2007;54:1333-1341.

57. Sevcik MA, Luger NM, Mach DB, et al. Bone cancer pain: the effects of the bisphosphonate alendronate on pain, skeletal remodeling, tumor growth and tumor necrosis. *Pain*. 2004;111:169-180.

58. Souza RB, Powers CM. Differences in hip kinematics, muscle strength, and muscle activation between subjects with and without patellofemoral pain. *J Orthop Sports Phys Ther*. 2009;39:12-19.

59. Stäubli HU, Schatzmann L, Brunner P, et al. Mechanical tensile properties of the quadriceps tendon and patellar ligament in young adults. *Am J Sports Med*. 1999;27:27-34.

60. Taddei F, Schileo E, Helgason B, et al. The material mapping strategy influences the accuracy of CT-based finite element models of bones: an evaluation against experimental measurements. *Med Eng Phys*. 2007;29:973-979.

61. Tennant S, Williams A, Vedi V, et al. Patello-femoral tracking in the weight-bearing knee: a study of asymptomatic volunteers utilising dynamic magnetic resonance imaging: a preliminary report. *Knee Surg Sports Traumatol Arthrosc*. 2001;9:155-162.

62. Toegel S, Hoffmann O, Wadsak W, et al. Uptake of bone-seekers is solely associated with mineralisation! A study with 99mTc-MDP, 153Sm-EDTMP and 18F-fluoride on osteoblasts. *Eur J Nucl Med Mol Imaging*. 2006;33: 491-494.

63. Tomiya M, Fujikawa K, Ichimura S, et al. Skeletal unloading induces a full-thickness patellar cartilage defect with increase of urinary collagen II CTx degradation marker in growing rats. *Bone*. 2009;44(2):295-305.

64. Van Tiggelen D, Cowan S, Coorevits P, et al. Delayed vastus medialis obliquus to vastus lateralis onset timing contributes to the development of patellofemoral pain in previously healthy men: a prospective study. *Am J Sports Med*. 2009;37:1099-1105.

65. Ward SR, Terk MR, Powers CM. Patella alta: association with patellofemoral alignment and changes in contact area

1032   during weight-bearing. *J Bone Joint Surg*. 2007;89-A:
1033   1749-1755.
1034   66. Witonski D, Wagrowska-Danielewicz M. Distribution of
1035   substance-P nerve fibers in the knee joint in patients with
1036   anterior knee pain syndrome. A preliminary report. *Knee*
1037   *Surg Sports Traumatol Arthrosc*. 1999;7:177-183.
1038   67. Witvrouw E, Sneyers C, Lysens R, et al. Reflex response
1039   times of vastus medialis oblique and vastus lateralis in

1040   normal subjects and in subjects with patellofemoral pain
1041   syndrome. *J Orthop Sports Phys Ther*. 1996;24:160-165.
1042   68. Wojtys EM, Beaman DN, Glover RA, et al. Innervation of
1043   the human knee joint by substance-P fibers. *Arthroscopy*.
1044   1990;6:254-263.
1045   69. Yamada Y, Toritsuka Y, Horibe S, et al. In vivo movement
1046   analysis of the patella using a three-dimensional computer
1047   model. *J Bone Joint Surg*. 2007;9-B:752-760.